Eur J Nucl Med Mol Imaging (2008) 35:798–807
DOI 10.1007/s00259-007-0668-y

ORIGINAL ARTICLE

Clinical performance and radiation dosimetry of no-carrier-added vs carrier-added ^{123}I-metaiodobenzylguanidine (MIBG) for the assessment of cardiac sympathetic nerve activity

Hein J. Verberne · Ellinor Busemann Sokole · Astrid F. van Moerkerken · Joop H. W. M. Deeterink · Geert Ensing · Michael G. Stabin · G. Aernout Somsen · Berthe L. F. van Eck-Smit

Received: 17 April 2007 / Accepted: 26 November 2007 / Published online: 4 January 2008

Abstract
Purpose We hypothesized that assessment of myocardial sympathetic activity with no-carrier-added (nca) ^{123}I-meta-iodobenzylguanidine (MIBG) compared to carrier-added (ca) ^{123}I-MIBG would lead to an improvement of clinical performance without major differences in radiation dosimetry.
Methods In nine healthy volunteers, 15 min and 4 h planar thoracic scintigrams and conjugate whole-body scans were performed up to 48 h following intravenous injection of 185 MBq ^{123}I-MIBG. The subjects were given both nca and ca ^{123}I-MIBG. Early heart/mediastinal ratios (H/M), late H/M ratios and myocardial washout were calculated. The fraction of administered activity in ten source organs was quantified from the attenuation-corrected geometric mean counts in conjugate views. Radiation-absorbed doses were estimated with OLINDA/EXM software.
Results Both early and late H/M were higher for nca ^{123}I-MIBG (ca ^{123}I-MIBG early H/M 2.46±0.15 vs nca ^{123}I-MIBG 2.84±0.15, p=0.001 and ca ^{123}I-MIBG late H/M 2.69±0.14 vs nca ^{123}I-MIBG 3.34±0.18, p=0.002). Myocardial washout showed a longer retention time for nca ^{123}I-MIBG (p<0.001). The effective dose equivalent (adult male model) for nca ^{123}I-MIBG was similar to that for ca ^{123}I-MIBG (0.025±0.002 mSv/MBq vs 0.026±0.002 mSv/MBq, p=0.055, respectively).
Conclusion No-carrier-added ^{123}I-MIBG yields a higher relative myocardial uptake and is associated with a higher myocardial retention. This difference between nca ^{123}I-MIBG and ca ^{123}I-MIBG in myocardial uptake did not result in major differences in estimated absorbed doses. Therefore, nca ^{123}I-MIBG is to be preferred over ca ^{123}I-MIBG for the assessment of cardiac sympathetic activity.

Keywords Cardiology · Heart failure · Sympathetic innervation · ^{123}I-MIBG · Dosimetry

H. J. Verberne (✉) · E. Busemann Sokole · A. F. van Moerkerken · J. H. W. M. Deeterink · B. L. F. van Eck-Smit
Department of Nuclear Medicine, Academic Medical Center, University of Amsterdam,
F2-238, P.O. Box 22700, 1100 DE Amsterdam, The Netherlands
e-mail: h.j.verberne@amc.uva.nl

G. Ensing
Mallinckrodt Medical, Tyco Healthcare BV,
Petten, The Netherlands

M. G. Stabin
Vanderbilt University,
Nashville, TN, USA

G. A. Somsen
Department of Cardiology, Onze Lieve Vrouwe Gasthuis,
Amsterdam, The Netherlands

Introduction

Meta-iodobenzylguanidine (MIBG), in analogy to catecholamines, is removed primarily from the circulation by sodium-driven, desipramine-sensitive, high-affinity transporters into the presynaptic noradrenergic neurons and stored in the presynaptic storage vesicles (called uptake 1) [1]. In addition, there is MIBG uptake by the corticosterone-sensitive, low-affinity, high-capacity, extra-neuronal transport system, originally named uptake 2 [2]. Uptake 1 predominates at

low concentrations of both catecholamines and MIBG, whereas uptake 2 predominates at higher concentrations [3]. Blocking experiments have shown that uptake 2 is responsible for up to 61% of myocardial MIBG uptake [4–8]. For routine clinical studies, the production of ^{123}I-MIBG involves isotopic exchange that gives a low specific activity (presence of a considerable amount of carrier, i.e., nonradio-labeled MIBG, in the final product) [9]. As uptake 2 predominates at higher concentration of MIBG, scintigraphic-determined semi-quantitative parameters will not improve by increasing the dose of ^{123}I-MIBG using a *relatively* low-specific-activity ^{123}I-MIBG compound. Increasing the dose of *relatively* low-specific-activity ^{123}I-MIBG might even lead to saturation of the uptake-1 mechanism. Reduction of the total amount of MIBG in combination with a higher specific activity (higher ratio radio-labeled/nonradio-labeled, i.e., no-carrier-added (nca) ^{123}I-MIBG), however, may favor myocardial uptake of ^{123}I-MIBG through uptake 1 [10]. In a blocking experiment (animal setting), we have shown that nca ^{123}I-MIBG leads to a better contrast between specific and nonspecific ^{123}I-MIBG uptake as compared to carrier-added (ca) ^{123}I-MIBG [11].

We hypothesized that the experimental differences in myocardial uptake of nca ^{123}I-MIBG compared to ca ^{123}I-MIBG observed in the animal studies should also be found in human subjects. This increase in myocardial uptake would lead to an improvement in the clinically relevant semi-quantitative parameters of myocardial ^{123}I-MIBG uptake [i.e., early heart/mediastinal ratios (H/M), late H/M ratios and myocardial washout]. In addition, we hypothesized that this improved myocardial uptake of nca ^{123}I-MIBG would not lead to any major differences in dosimetry. In the present study, we evaluated the intra-individual differences of clinical performance and radiation dosimetry for both nca ^{123}I-MIBG and ca ^{123}I-MIBG.

Materials and methods

Study protocol

Healthy volunteers were injected with approximately 185 MBq of ca ^{123}I-MIBG and with approximately 185 MBq of nca ^{123}I-MIBG on two separate days with a 2-week interval. To minimize the possibility of order bias, five of the subjects received first ca ^{123}I-MIBG followed by nca ^{123}I-MIBG, and in the other four subjects, the order was reversed. After injection, images were obtained for the assessment of clinically relevant parameters of MIBG and also for calculation of radiation dosimetry. The study protocol was approved by the institutional Medical Ethics Committee.

Study group

Nine healthy volunteers (four women and five men), with a mean age of 29 years (range 21–59 years) and a low likelihood of coronary artery disease (<5%), were included after they had given their written informed consent. The subjects were free of disease based on screening by medical history and physical examination. None of the subjects used any medication that could interfere with ^{123}I-MIBG uptake. Each subject received approximately 200 mg potassium iodide (10% solution) orally, taken as three daily fractionated doses on the day before and on the day of injection, to block thyroid uptake of free radioactive iodide.

Radiopharmaceuticals

No-carrier-added ^{123}I-MIBG was produced via the well-established Cu(I)-catalyzed nonisotopic (^{123}I/Br) exchange reaction in an acidic, aqueous medium [12]. A reproducible and high labeling yield (70–80%, approximately 5–6 GBq nca ^{123}I, at the time of synthesis; Na^{123}I from Mallinckrodt Medical, Tyco Healthcare BV, Petten, The Netherlands) was obtained, and final reaction mixture was injected into a semi-preparative high-performance liquid chromatography (HPLC) system (using an isotonic EtOH/acetate eluent) to separate the radio-iodinated ^{123}I-MIBG from its brominated precursor. A second HPLC separation was performed on the first collected fraction to obtain nca ^{123}I-MIBG, free from pseudo-carrier (bromo-precursor). The ultimate collected nca ^{123}I-MIBG was further diluted with an isotonic citrate buffer (pH 5), filtrated, dispensed and sterilized by autoclavation. The radiochemical purity of the autoclaved nca ^{123}I-MIBG was higher than 98% (30 h after synthesis), with an overall yield of 55–65%. Postproduction UV-HPLC analyses of the final product showed complete absence of bromo-precursor. No-carrier-added ^{123}I-MIBG had a specific activity in the order of 1,700 GBq/μmol MIBG.

Carrier-added ^{123}I-MIBG was produced according to an isotopic exchange procedure and had a radiochemical purity of more than 97% and a specific activity in the order of 40 MBq/μmol MIBG. By comparison, the difference in specific activity between nca ^{123}I-MIBG and ca ^{123}I-MIBG was more than a factor of 10.000. The specific radioactivity of ca ^{123}I-MIBG can therefore be considered to be low but is that encountered in current routine clinical practice.

Instrumentation

All images were obtained with a dual-head scintillation camera (E.cam, Siemens, Germany) fitted with medium energy collimators. A 15% energy window was used for ^{123}I and ^{57}Co. The medium energy collimators provided minimum septum penetration of the higher energy photons

of the ^{123}I radionuclide [13]. All whole-body scans, both emission and transmission, were obtained in anterior and posterior views with a scan speed of 8 cm/min. All measurements were obtained in each subject for both ca ^{123}I-MIBG and nca ^{123}I-MIBG. The same radionuclide dose calibrator was used for all ^{123}I activity measurements.

Semi-quantitative ^{123}I-MIBG myocardial indices

At 15 min and 4 h post-injection of ^{123}I-MIBG, 10 min anterior planar acquisitions were made of the thorax. Images were made with a 256×256 matrix size, using the settings described above.

Whole-body emission scans

For each subject, a series of six whole-body emission scans were obtained at 30 min, 1.5, 2.5, 4.5, 6 and 24 h post-injection of ^{123}I-MIBG. In two subjects, whole-body scans were also obtained at 48 h. The stability of these measurements over the total measurement period was monitored by including a vial containing 2 MBq of ^{123}I placed between the lower legs of the subject during each emission scan.

A quality control check of the equality of the sensitivity of anterior and posterior collimated detectors for ^{123}I was verified, according to the NEMA NU-1 protocol [14]. The calibration factor applied to convert whole-body counts to MBq was measured and monitored for the anterior detector head. This calibration factor gave the conversion of counts to MBq measured in air, without absorption of the imaging pallet. Because of interference of the imaging pallet, a similar measurement in air for the posterior detector head was not possible. This factor was obtained from a whole-body scan of the Petri dish, containing an amount of ^{123}I (25 MBq) exactly calibrated in the radionuclide dose calibrator, placed on the imaging table. The net counts were obtained from a circular region of interest (ROI) over the Petri dish image and a copy of the circular ROI placed in a background region. The activity was calibrated to the actual time of scanning over the Petri dish.

Whole-body transmission imaging

For the purpose of attenuation correction, a dual-head whole-body transmission scan was obtained for each subject before ^{123}I MIBG injection. A 300 MBq ^{57}Co flood source was placed on the lower detector head. The upper detector head thus measured transmission through the patient and imaging table in anterior view, whereas the lower detector measured counts in air. In the dosimetry calculations, a correction was made for the difference in attenuation between ^{57}Co and ^{123}I using a measured linear broad-beam attenuation factor of 0.145 cm^{-1} ^{57}Co and 0.138 cm^{-1} for ^{123}I.

Blood and urine

Blood samples were obtained at 10 min, 1 h and subsequently directly before each whole-body scan. Three duplicate 1 ml samples of blood were measured in a gamma sample changer with an appropriate standard ^{123}I activity to convert from counts to MBq. Total amount of radioactivity in the blood was calculated using a total blood volume based on gender and individual body weight and height and expressed as % injected dose of ^{123}I-MIBG [15–17].

Urine was collected to verify excretion kinetics. The urine was collected in separate containers corresponding to separate collection periods. The first collection period started directly after injection of ^{123}I-MIBG and was completed after the first whole-body scan. The subsequent collection periods ended before each successive whole-body scan. This gave five containers up to 24 h and six containers up to 48 h. The urine volume in each container was determined by the net weight of each urine container. Three duplicate 1 ml samples from each container were measured in the gamma sample changer and the total urine activity estimated using the total urine volume from each collection period.

Image analysis—semi-quantitative ^{123}I-MIBG myocardial indices

An experienced nuclear medicine technologist (AvM), blind to the radiopharmaceutical used, processed all planar images (HERMES workstation, Nuclear Diagnostics, Stockholm, Sweden). A ROI for myocardial activity was manually drawn and included both ventricles and atrial activity, if observed. A fixed rectangular mediastinal ROI (100 pixels) was drawn in the upper mediastinum, using the apices of the lungs as anatomic landmarks (Fig. 1). The H/M (early and late) was calculated as the ratio of the counts/pixel in the two ROIs. Myocardial washout was calculated as:

$$\left\{\frac{(\text{earlyH/M} - \text{lateH/M})}{\text{earlyH/M}}\right\} \times 100\%$$

and myocardial retention was calculated as:

$$\left\{\frac{\text{earlyH} - \text{lateH}^{\text{dc}}}{\text{earlyH}}\right\} \times 100\%$$

where late H^{dc} stands for late H decay corrected. The calculation of myocardial retention implies that the lower the outcome (i.e., lesser myocardial washout), the higher the myocardial retention.

Image analysis—whole-body scans

For each subject, an anterior and posterior set of ROIs was created for the activity observed in the source organs of

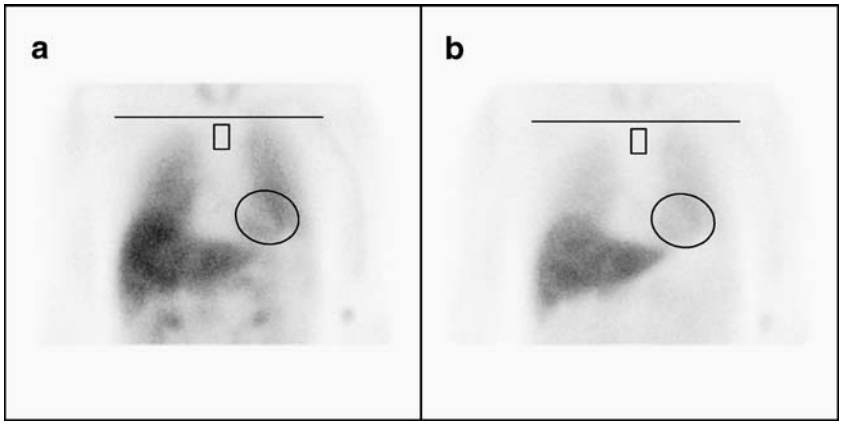

Fig. 1 Example of processing procedure for early (**a**) and late (**b**) planar ^{123}I-MIBG images. The positioning of the mediastinal ROI was standardized in relation to the lung apex, the lower boundary of the upper mediastinum and the midline between the lungs

interest: liver, myocardium, lungs, kidneys, spleen, thyroid, bladder, submandibular and parotid glands, intestines and over the total body. The anterior lung ROI was obtained from the anterior ^{57}Co transmission scan. Different background (BG) ROIs were also obtained and applied to the various organ ROIs: groin (BG correction for liver, kidneys, bladder, spleen, intestines), mediastinum (BG correction for myocardium), thigh (BG correction for thyroid), head (BG correction for submandibular and parotid glands) and outside the body ROI (BG correction for whole-body ROI). The anterior and posterior ROIs mirrored each other. Once a set of anterior and posterior ROIs had been created, this set was applied to each whole-body scan of the ca ^{123}I MIBG and nca ^{123}I MIBG studies, including the transmission scans. Adjustment was applied when necessary for a difference in position of the patient. The counts and pixels in each ROI were obtained (HERMES Medical Solutions, Stockholm, Sweden).

For each emission whole-body scan, organ counts were corrected for their appropriate BG counts. The ^{57}Co attenuation correction factor for each organ was obtained from the square root of the ratio (anterior counts per pixel/posterior counts per pixel) in the transmission scan. This ^{57}Co attenuation factor was then corrected to ^{123}I attenuation using the measured broad beam linear attenuation factors. The attenuated corrected counts were ultimately converted to MBq and percentage of injected activity. To obtain biological kinetics, a decay correction was applied, using the time between injected activity and start of the whole-body scan, plus an extra 10 min, as the decay time interval.

Dosimetry

The OLINDA/EXM software was used to obtain absorbed doses [18]. This software includes a kinetic input module for determining organ residence times. The residence times for the source organs were obtained using the OLINDA/EXM kinetic input model, applying a two- or three-exponential fit to the data of each source organ. The whole-body retention data, whereby the geometric mean counts in the first scan was set equal to 100% of injected activity, corresponded with the accumulated activity excreted in the urine. The whole-body data were therefore used to calculate the total body residence time and also formed the basis for the kinetics of the urinary bladder contents. The blood activity was input into the remainder body organ of OLINDA/EXM. The difference between the total number of disintegrations in total body and in the sum of all source organs, excluding the urinary bladder contents, was applied to the muscle as a source organ. The number of disintegrations in urinary bladder contents was calculated based on the whole-body excretion (two-exponential component fit) and assuming a 4-h bladder voiding interval. The self-dose to the salivary glands was estimated using the OLINDA/EXM sphere model. The OLINDA/EXM software estimates intestinal absorbed dose only on the basis of intra-luminal activity and does not correct for intestine self-dose. However the intestine is a sympathetically innervated organ [19, 20]. A subsequent correction was made to the beta-component of the absorbed dose estimate for the intestinal wall. The radiation dose estimates were calculated for each subject independently and then averaged. Separate sets of values were generated for the OLINDA/EXM adult male and adult female input models. All calculations were based on the assumption that the product contained 100% pure ^{123}I.

Statistical analysis

Normal distribution was assessed by the Kolmogorov–Smirnov test. In the case of normal distribution, mean differences were compared with a paired Student's t test. In the case of abnormal distribution, means were compared with the Wilcoxon rank test (SPSS for Windows 11.5.1, SPSS, Chicago, IL, USA). A p value <0.05 was considered

to indicate a statistically significant difference. Unless indicated otherwise, data are expressed as mean±standard deviation (SD).

Results

Semi-quantitative ^{123}I-MIBG myocardial indices

Figure 2 shows the clinically relevant semi-quantitative ^{123}I-MIBG indices. Both early and late H/M (Fig. 2a and b) were higher for nca ^{123}I-MIBG (early ca ^{123}I-MIBG H/M=2.46±0.15 vs nca ^{123}I-MIBG=2.84±0.15, p=0.001; and late ca ^{123}I-MIBG H/M=2.69±0.14 vs nca ^{123}I-MIBG=3.34±0.18, p=0.002). The myocardial washout (Fig. 2c) showed a trend towards a higher myocardial uptake over time (negative myocardial washout) for nca ^{123}I-MIBG (ca ^{123}I-MIBG=−10.85±4.40% vs nca ^{123}I-MIBG=−18.04±4.31%). This trend, however, was statistically not significant (p=0.128). In contrast, nca ^{123}I-MIBG showed a higher myocardial retention (Fig. 2d; i.e., lower myocardial washout) of 47% compared to ca ^{123}I-MIBG (ca ^{123}I-MIBG=23.07±2.29% vs nca ^{123}I-MIBG=12.20±3.96%, p=0.003).

Dosimetry

Whole-body images of one subject, showing the biodistribution of radioactivity after intravenous injection of ^{123}I-MIBG at different time points post-injection, are presented in Fig. 3. The uptake pattern was already established at 30 min after injection, with definite uptake seen in the myocardium, lungs, liver, intestines, submandibular and parotid glands. Excretion to the urinary bladder was already present by 30 min. No major changes in distribution over time were observed up to 48 h after injection of ^{123}I-MIBG. Figure 4 shows the average time-activity curves obtained for the myocardium, lungs, liver and total body. Although the time activity curve of the myocardial wall for nca ^{123}I-MIBG was higher compared to that of ca ^{123}I-MIBG (statistically significant for all time points), there was no difference in the washout rate between ca ^{123}I-MIBG and nca ^{123}I-MIBG (Fig. 4a). The lungs and liver showed no variation between ca ^{123}I-MIBG and nca ^{123}I-MIBG (Fig. 4b and c). The total body showed a trend towards slightly higher retention for nca ^{123}I-MIBG compared to ca ^{123}I-MIBG (Fig. 4d).

Table 1 gives the number of disintegrations (MBq-h/MBq administered) for the different source organs. The

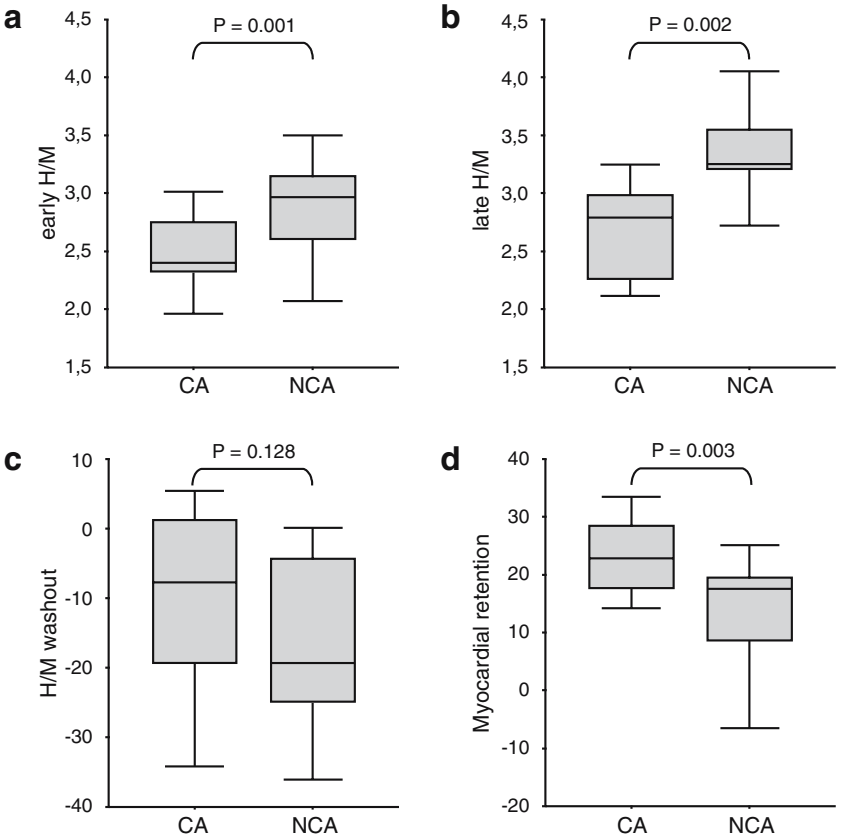

Fig. 2 Comparison of clinical performance of ca ^{123}I-MIBG vs nca ^{123}I-MIBG. Early and late H/M were higher for nca ^{123}I-MIBG (**a** and **b** p=0.001 and p=0.002, respectively). Although myocardial retention for nca ^{123}I-MIBG (**d**) improved (p=0.003), the clinically used myocardial washout showed no difference (**c**)

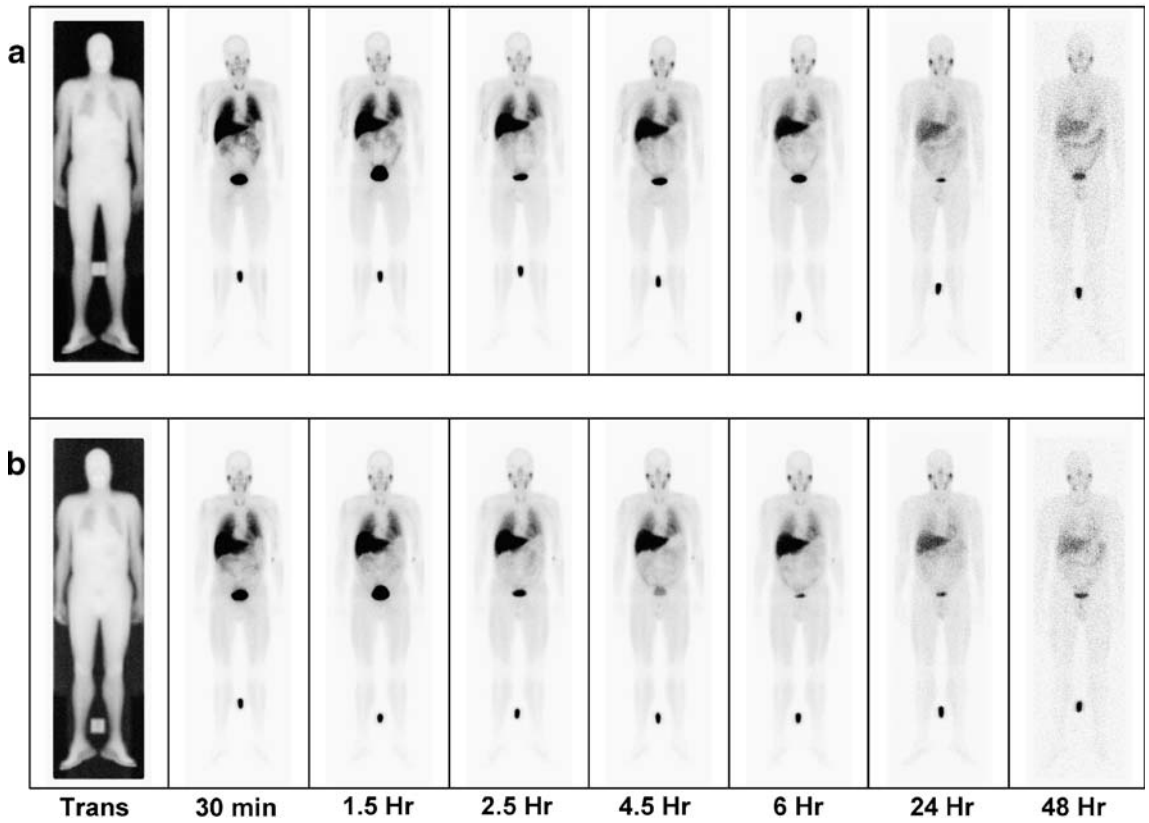

Fig. 3 Anterior whole-body transmission (Trans) scan (obtained before injection of ^{123}I-MIBG) and anterior whole-body emission images obtained from a 58-year-old male volunteer at several time points after administration of ca ^{123}I-MIBG (**a**) and of nca ^{123}I-MIBG (**b**). In this volunteer, the first voiding period after injection took place after the second whole-body emission scan instead of the first whole-body emission scan. A holder (seen on the transmission scan) for the ^{123}I-standard (seen on the emission scans) was placed between the lower legs of the volunteer(s)

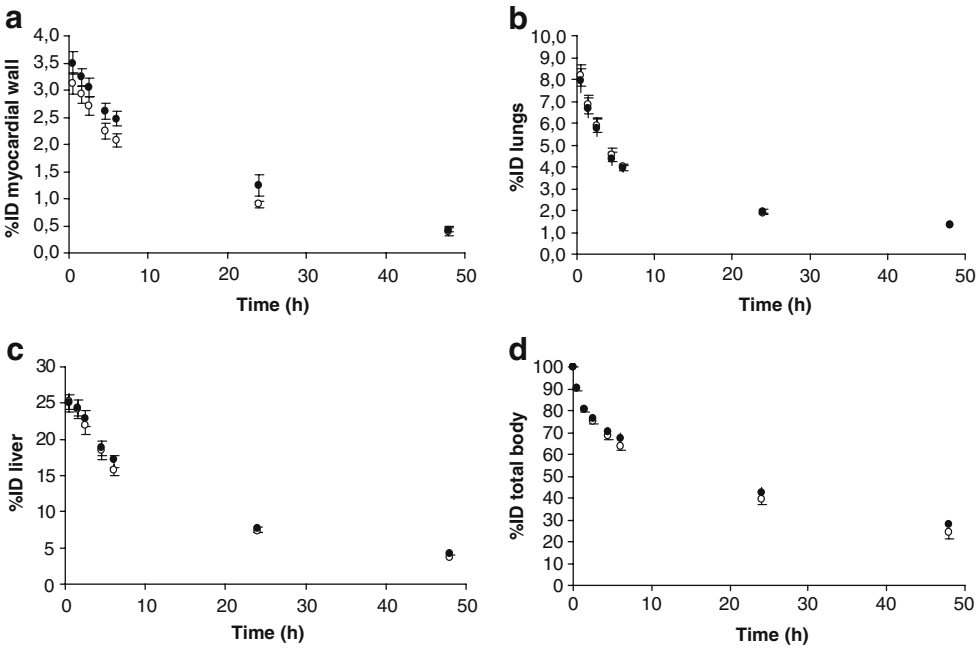

Fig. 4 Time activity curves for myocardial wall (**a**), lungs (**b**), liver (**c**), and total body (**d**) of ca ^{123}I-MIBG (*open circles*) and of nca ^{123}I-MIBG (*closed circles*). Data are expressed as the averaged (*circles*) and the standard error (*bars*) % injected dose (% ID) for the nine subjects

Table 1 Number of disintegrations (MBq-h/MBq administered) for ca ^{123}I-MIBG and nca ^{123}I-MIBG for total body and each source organ

	ca ^{123}I-MIBG Mean±SD	nca ^{123}I-MIBG Mean±SD	*p* value
Total body	9.812±1.022	10.392±0.964	0.001
Salivary glands	0.122±0.025	0.123±0.035	0.964
Lower large intestine	0.442±0.070	0.440±0.062	0.881
Upper large intestine	0.442±0.070	0.440±0.062	0.881
Myocardial wall	0.290±0.051	0.360±0.083	0.017
Kidneys	0.248±0.071	0.259±0.078	0.504
Liver	2.330±0.516	2.433±0.410	0.236
Lungs	0.616±0.127	0.621±0.129	0.853
Muscle	5.000±0.881	5.424±0.890	0.010
Spleen	0.089±0.030	0.090±0.041	0.915
Thyroid	0.035±0.008	0.044±0.020	0.108
Urinary Bladder Contents	1.130±0.147	1.079±0.141	0.019
Remainder	0.196±0.033	0.182±0.033	0.054

The *p* values are obtained from paired individual results.

average number of disintegrations in total body for nca ^{123}I-MIBG was higher than that for ca ^{123}I-MIBG. Moreover, nca ^{123}I-MIBG showed higher numbers of disintegrations for myocardium and muscle. The number of disintegrations for urinary bladder contents was lower for nca ^{123}I-MIBG, indicating a slightly lesser excretion for nca ^{123}I-MIBG. The number of disintegrations for both ca ^{123}I-MIBG as for nca ^{123}I-MIBG was highest for muscle, followed by liver and urinary bladder contents.

Table 2 displays the averaged estimated absorbed doses for the OLINDA/EXM adult male and female models for ca ^{123}I-MIBG and nca ^{123}I-MIBG The organs that received the highest absorbed doses for both ca ^{123}I-MIBG as for nca ^{123}I-MIBG were the urinary bladder wall (based on a 4-h voiding interval), followed by the lower large intestine, upper large intestine, liver and myocardial wall (Table 2). Dose to the myocardial wall was notably higher for the nca ^{123}I-MIBG, as would be expected based on the biokinetics. The absorbed doses per organ for females were higher compared to males for both ca ^{123}I-MIBG as for nca ^{123}I-MIBG. The mean effective dose equivalent for the normal male adult for ca ^{123}I-MIBG was of the same order of magnitude as for nca ^{123}I-MIBG (p=0.055). The mean effective dose equivalent for the normal female adult for ca ^{123}I-MIBG was slightly lower compared to nca ^{123}I-MIBG (p=0.026). The effective dose equivalent and effective dose in females was, for both ca ^{123}I-MIBG and nca ^{123}I-MIBG, higher compared to males (p<0.001; Table 2).

Discussion

The main goal of this study was to test whether the experimental differences, noted in animal studies, in myocardial uptake of nca ^{123}I-MIBG compared to ca ^{123}I-MIBG would also be seen in human subjects, without major changes in dosimetry. Our findings indicate that, in general, nca ^{123}I-MIBG yields a higher relative myocardial uptake compared to ca ^{123}I-MIBG (25%). The difference between nca ^{123}I-MIBG and ca ^{123}I-MIBG in myocardial uptake did not result in major differences in estimated effective dose equivalents or effective doses.

Semi-quantitative ^{123}I-MIBG myocardial indices

The observed higher myocardial uptake of nca ^{123}I-MIBG as compared with ca ^{123}I-MIBG in humans is in line with previous studies. This difference was explained by a longer myocardial retention time (i.e., negative myocardial washout) for nca ^{123}I-MIBG. Farahati et al. were the first to report the use of nca ^{123}I-MIBG for myocardial scintigraphy in humans. In a limited number of healthy volunteers (n=3), planar-assessed nca ^{123}I-MIBG showed an increase in relative myocardial uptake compared with ca ^{123}I-MIBG. However, nca ^{123}I-MIBG images were not superior to ca ^{123}I-MIBG [21]. The authors related this lack in superiority to in vivo deiodination, which resulted in higher background activity. However, in patients with ventricular arrhythmias, Samnick et al. [22] showed that the relative myocardial uptake of nca ^{123}I-MIBG as assessed with single-photon emission computed tomography was higher than myocardial uptake of ca ^{123}I-MIBG. These findings were similar to those reported in another cohort of patients evaluated for tachyarrhythmia [23]. However, in none of these studies, clinically relevant parameters of myocardial ^{123}I-MIBG uptake (i.e., early H/M, late H/M ratios and myocardial washout) were reported. In addition, the study of Knickmeier et al. [23] made a comparison between different patient groups, and no direct comparison was made between nca ^{123}I-MIBG and ca ^{123}I-MIBG within the same patient.

Table 2 Radiation-absorbed estimates (mSv/MBq) for ^{123}I-MIBG

	ca ^{123}I-MIBG		nca ^{123}I-MIBG	
	Men Mean±SD	Women Mean±SD	Men Mean±SD	Women Mean±SD
Adrenals	1.08E-02±1.31E-03	1.34E-02±1.61E-03	1.13E-02±8.91E-04	1.41E-02±1.18E-03
Brain	7.69E-04±9.91E-05	7.98E-04±1.02E-04	8.01E-04±1.04E-04	8.25E-04±1.12E-04
Breasts	3.08E-03±3.18E-04	3.82E-03±3.80E-04	3.29E-03±2.72E-04	4.08E-03±3.42E-04
Gallbladder wall	1.68E-02±2.46E-03	2.08E-02±3.01E-03	1.75E-02±1.62E-03	2.17E-02±2.12E-03
Lower large intestine wall	5.94E-02±8.13E-03	6.51E-02±8.76E-03	5.93E-02±6.91E-03	6.50E-02±7.89E-03
Small intestine	1.04E-02±8.80E-04	1.31E-02±1.10E-03	1.06E-02±7.82E-04	1.34E-02±1.03E-03
Stomach wall	6.88E-03±6.60E-04	9.05E-03±8.73E-04	7.27E-03±6.30E-04	9.55E-03±8.16E-04
Upper large intestine wall	4.76E-02±6.68E-03	5.29E-02±7.39E-03	4.76E-02±5.58E-03	5.30E-02±6.46E-03
Heart wall	2.91E-02±3.93E-03	3.76E-02±5.05E-03	3.48E-02±5.98E-03	4.49E-02±8.15E-03
Kidneys	2.90E-02±6.65E-03	3.26E-02±7.30E-03	3.04E-02±6.73E-03	3.41E-02±7.80E-03
Liver	5.01E-02±1.03E-02	6.49E-02±1.33E-02	5.23E-02±7.47E-03	6.78E-02±1.03E-02
Lungs	2.07E-02±3.44E-03	2.70E-02±4.44E-03	2.13E-02±3.08E-03	2.78E-02±4.24E-03
Muscle	8.60E-03±9.11E-04	1.18E-02±1.29E-03	9.14E-03±8.97E-04	1.25E-02±1.34E-03
Ovaries	na	1.58E-02±1.00E-03	na	1.60E-02±1.02E-03
Pancreas	1.03E-02±1.15E-03	1.33E-02±1.52E-03	1.09E-02±8.82E-04	1.40E-02±1.20E-03
Red marrow	5.06E-03±4.22E-04	6.13E-03±5.07E-04	5.30E-03±3.94E-04	6.42E-03±5.06E-04
Osteogenic cells	8.45E-03±8.05E-04	1.07E-02±1.02E-03	8.90E-03±7.82E-04	1.12E-02±1.02E-03
Skin	2.72E-03±2.64E-04	3.31E-03±3.17E-04	2.87E-03±2.52E-04	3.50E-03±3.28E-04
Spleen	1.88E-02±4.85E-03	2.31E-02±5.83E-03	1.93E-02±6.25E-03	2.37E-02±7.96E-03
Testes	5.06E-03±3.01E-04	na	5.19E-03±2.83E-04	na
Thymus	5.67E-03±5.46E-04	6.95E-03±6.80E-04	6.21E-03±5.63E-04	7.57E-03±7.27E-04
Thyroid	3.85E-02±7.92E-03	4.58E-02±9.49E-03	4.76E-02±1.90E-02	5.67E-02±2.43E-02
Urinary bladder wall	8.63E-02±9.99E-03	1.27E-01±1.50E-02	8.32E-02±8.86E-03	1.23E-01±1.42E-02
Uterus	na	1.65E-02±5.87E-04	na	1.66E-02±5.02E-04
Total body	8.49E-03±7.21E-04	1.02E-02±8.60E-04	8.95E-03±6.25E-04	1.08E-02±7.51E-04
Effective dose equivalent (mSv/MBq)	2.48E-02±1.47E-03[a]	3.14E-02±1.78E-03[c]	2.59E-02±1.63E-03	3.28E-02±1.34E-03
Effective dose (mSv/MBq)	2.87E-02±2.49E-03[b]	3.53E-02±2.87E-03[d]	2.94E-02±1.69E-03	3.60E-02±2.00E-03

na Not applicable
[a] ca male vs nca male $p=0.055$
[b] ca male vs nca male $p=0.181$
[c] ca female vs nca female $p=0.026$
[d] ca female vs nca female $p=0.177$

Therefore, differences between nca ^{123}I-MIBG and ca ^{123}I-MIBG myocardial uptake may have been blunted by regression to the mean. Although Faharati et al. reported on dosimetry of nca ^{123}I-MIBG, data on radiation-absorbed dose estimates were only obtained in one healthy subject.

The negative myocardial washout (Fig. 4c) is indicative of a higher myocardial uptake over time (Fig. 4d). This finding is in line with previous studies in healthy volunteers [24] and is probably an indication of a low myocardial sympathetic activity. In addition, the negative myocardial washout may (to some extent) be explained by a slower myocardial washout compared to mediastinal washout.

Dosimetry

Data on radiation absorbed dose estimates for MIBG (^{123}I or ^{131}I) in human subjects are limited and are based on publications from the early 1980s [25]. The International Commission on Radiological Protection (ICRP) publication 53 presents estimates of the biokinetic model based on these early data [26]. In the subsequent addenda to this ICRP publication (ICRP publication 80, based on some assumptions from ICRP publication 60), absorbed dose estimates for MIBG changed due to new assumptions in specific absorbed fractions to calculate the *S* values [27, 28].

Although a comparison between the early study of Jacobsson et al. [25] and our study reveals significant methodological differences (e.g., correction for attenuation, the number of time points studied), their effective dose estimates based on measurements with ^{131}I-MIBG are of the same order of magnitude as those presented here. However, the higher absorbed dose estimate in our study is probably related to differences in the standard input models and methods used to calculate estimated absorbed doses (OLINDA/EXM).

Our biodistribution data showed intestinal activity already in the early images. This is a reflection of the sympathetic

intestinal activity. Sympathetic nerve fibers enter the intestinal wall along arteries and terminate in the mesenteric and submucosal plexuses and in the mucosa [19, 20]. It is important to mention that sympathetic nerve fibers not only terminate in vessel walls or enteric plexuses to control vascular tone or secretomotor neurons but also end in the larger vicinity of blood vessels in the submucosa and mucosa. With respect to the gut-associated lymphoid tissue, represented by the appendix and Peyer's patches, sympathetic noradrenergic nerve fibers innervate both the vasculature and parenchymal fields of lymphocytes [20]. The OLINDA/EXM software estimates intestinal absorbed dose only on basis of intra-luminal activity and does not allow direct calculation of dose from intestinal wall to intestinal wall. Doses given by the software were manually corrected, retaining the photon dose contribution but correcting the electron dose contribution to reflect the appropriate target mass (details not shown).

There were relatively small differences in radiation-absorbed dose estimates between ca ^{123}I-MIBG and nca ^{123}I-MIBG. The difference between male and female dose estimates are related to the OLINDA/EXM input model based on a 73 kg adult male and 57 kg adult female model. The calculated radiation-absorbed dose estimates for both ca ^{123}I-MIBG and nca ^{123}I-MIBG remain well within the range of doses acceptable in clinical nuclear medicine studies. Based on an averaged (male and female model) effective dose equivalent of 0.03 mSv/MBq derived from the results of this study, both patients and human volunteers could be investigated with amounts of up to 185 MBq, which gives an average effective dose equivalent of approximately 5.6 mSv. In a 1988 publication, an average effective dose equivalent per patient from nuclear medicine procedures of 5 mSv was reported in Europe [29]. In a more recent publication from the USA, there is a tendency to a higher averaged effective dose equivalent per nuclear medicine procedure, up to 10 mSv [30]. With respect to human volunteers, the average effective dose equivalent fell well within the range of 1 and 10 mSv of category IIb of ICRP publication 62 [31]. This is considered an acceptable risk for volunteers.

Approximately 35% of injected ^{123}I-MIBG was excreted by 6 h, with excretion starting within 30 min after injection. Due to this rapid urinary excretion, frequent voiding is to be recommended to minimize the absorbed dose, especially to the urinary bladder wall but also to the gonads and other urinary bladder surrounding tissues.

Future perspective

Application of the semi-quantitative parameters of myocardial ^{123}I-MIBG uptake for prognostic assessment of patients with heart failure shows promise. However, estimates of the hazard ratio among studies differ substantially. This is reflected in the absence of ^{123}I-MIBG in any of the current guidelines regarding either heart failure or myocardial scintigraphic imaging [32–36]. To apply uniform prognostic threshold values, unequivocal methods for obtaining semi-quantitative parameters of myocardial ^{123}I-MIBG uptake have as yet to be established.

It is conceivable that the substantially higher myocardial uptake with nca ^{123}I-MIBG will lead to a lower variability and therefore to a better correlation with other (clinical) parameters of heart failure. In line with this, it is to be expected that, compared to ca ^{123}I-MIBG, nca ^{123}I-MIBG may perform better in the assessment of prognosis. However, this remains subject for future studies.

Conclusion

No-carrier-added ^{123}I-MIBG yields a higher relative myocardial uptake and is associated with a higher myocardial retention. The difference between nca ^{123}I-MIBG and ca ^{123}I-MIBG in myocardial uptake did not result in major differences in estimated absorbed dose. For the assessment of cardiac sympathetic activity, nca ^{123}I-MIBG is therefore to be preferred over ca ^{123}I-MIBG.

References

1. Pacholczyk T, Blakely RD, Amara SG. Expression cloning of a cocaine- and antidepressant-sensitive human noradrenaline transporter. Nature 1991;350:350–4.
2. Iversen LL. The uptake of cathecholamines at high perfusion concentrations in the rat isolated heart: a novel cathecholamine uptake process. Br J Pharmac Chemother 1965;25:18–33.
3. DeGrado TR, Zalutsky MR, Vaidyanathan G. Uptake mechanisms of meta-[123I]iodobenzylguanidine in isolated rat heart. Nucl Med Biol 1995;22:1–12.
4. Sisson JC, Shapiro B, Meyers L, Mallette S, Mangner TJ, Wieland DM, et al. Metaiodobenzylguanidine to map scintigraphically the adrenergic nervous system in man. J Nucl Med 1987;28:1625–36.
5. Sisson JC, Wieland DM, Sherman P, Mangner TJ, Tobes MC, Jacques S Jr. Metaiodobenzylguanidine as an index of the adrenergic nervous system integrity and function. J Nucl Med 1987;28:1620–4.
6. Rabinovitch MA, Rose CP, Schwab AJ, Fitchett DH, Honos GN, Stewart JA, et al. A method of dynamic analysis of iodine-123-metaiodobenzylguanidine scintigrams in cardiac mechanical overload hypertrophy and failure. J Nucl Med 1993;34:589–600.
7. Dae MW, O'Connell JW, Botvinick EH, Ahearn T, Yee E, Huberty JP, et al. Scintigraphic assessment of regional cardiac adrenergic innervation. Circulation 1989;79:634–44.
8. Fagret D, Wolf JE, Vanzetto G, Borrel E. Myocardial uptake of metaiodo-benzylguanidine in patients with left ventricular hypertrophy secondary to valvular aortic stenosis. J Nucl Med 1993; 34:57–60.
9. Mangner TJ, Wu JL, Wieland DM. Solid-phase exchange radioiodination of aryl iodides. Facilitation by ammonium sulfate. J Org Biochem 1982;47:1484–8.
10. Vaidyanathan G, Zalutsky MR. No-carrier-added meta-[123I] iodo-benzylguanidine: synthesis and preliminary evaluation. Nucl Med Biol 1995;22:61–4.

11. Verberne HJ, de Bruin K, Habraken JB, Somsen GA, Eersels JL, Moet F, et al. No-carrier-added versus carrier-added123I-metaiodobenzylguanidine for the assessment of cardiac sympathetic nerve activity. Eur J Nucl Med Mol Imaging 2006;33:483–90.
12. Eersels JHL, Travis MJ, Herscheid JDM. Manufacturing I-123-labelled radiopharmaceuticals. Pitfalls and solutions. J Label Comp Radiopharm 2005;48:241–257.
13. Verberne HJ, Feenstra C, de Jong WM, Somsen GA, van Eck-Smit BL, Busemann Sokole E. Influence of collimator choice and simulated clinical conditions on 123I-MIBG heart/mediastinum ratios: a phantom study. Eur J Nucl Med Mol Imaging 2005;32:1100–7.
14. Performance Measurements of Scintillation Cameras, NEMA Standards. Publications NU 1. 1994.
15. Du Bois D, Du Bois EF. A formula to estimate the approximate surface area if height and weight be known. Arch Intern Med 1916;17:863–71.
16. Brown E, Hopper J Jr., Hodges JL Jr., Bradley B, Wennesland R, Yamauchi H. Red cell, plasma, and blood volume in the healthy women measured by radiochromium cell-labeling and hematocrit. J Clin Invest 1962;41:2182–90.
17. Wennesland R, Brown E, Hopper J Jr., Hodges JL Jr., Guttentag OE, Scott KG, et al. Red cell, plasma and blood volume in healthy men measured by radiochromium (Cr51) cell tagging and hematocrit: influence of age, somatotype and habits of physical activity on the variance after regression of volumes to height and weight combined. J Clin Invest 1959;38:1065–77.
18. Stabin MG, Sparks RB, Crowe E. OLINDA/EXM: the second-generation personal computer software for internal dose assessment in nuclear medicine. J Nucl Med 2005;46:1023–7.
19. Furness JB. The origin and distribution of adrenergic nerve fibres in the guinea-pig colon. Histochemie 1970;21:295–306.
20. Felten DL, Felten SY, Carlson SL, Olschowka JA, Livnat S. Noradrenergic and peptidergic innervation of lymphoid tissue. J Immunol 1985;135:755s–65s.
21. Farahati J, Bier D, Scheubeck M, Lassmann M, Schelper LF, Grelle I, et al. Effect of specific activity on cardiac uptake of iodine-123-MIBG. J Nucl Med 1997;38:447–51.
22. Samnick S, Bader JB, Muller M, Chapot C, Richter S, Schaefer A, et al. Improved labelling of no-carrier-added 123I-MIBG and preliminary clinical evaluation in patients with ventricular arrhythmias. Nucl Med Commun 1999;20:537–45.
23. Knickmeier M, Matheja P, Wichter T, Schafers KP, Kies P, Breithardt G, et al. Clinical evaluation of no-carrier-added meta-[123I]iodobenzylguanidine for myocardial scintigraphy. Eur J Nucl Med 2000;27:302–7.
24. Somsen GA, Verberne HJ, Fleury E, Righetti A. Normal values and within-subject variability of cardiac I-123 MIBG scintigraphy in healthy individuals: implications for clinical studies. J Nucl Cardiol 2004;11:126–33.
25. Jacobsson L, Mattson S, Johansson L, Lindberg S, Fjälling M. Biokinetics and dosimetry of 131I-metaiodobenzylguanidine (MIBG). Proceedings of the Fourth International Radiopharmaceutical Dosimetry Symposium. Oak Ridge 1985. Oak Ridge National Laborotories, Oak Ridge, Tennessee: Oak Ridge Assoc. Universities CONF-851113; 1986. p. 389–98.
26. Radiation dose to patients from radiopharmaceuticals. A report of a Task Group of Committee 2 of the International Commission on Radiological Protection. Ann ICRP 1987;18:1–377.
27. Valentin J. Radiation dose to patients from radiopharmaceuticals: (Addendum 2 to ICRP Publication 53) ICRP Publication 80 Approved by the Commission in September 1997. Ann ICRP 1998;28:1–121.
28. International Commission on Radiological Protection. Recommendations of the International Commission on Radiological Protection. ICRP Publication 60. Oxford: Pergamon Press; 1991.
29. Beekhuis H. Population radiation absorbed dose from nuclear medicine procedures in The Netherlands. Health Phys 1988;54:287–91.
30. Ngutter LK, Kofler JM, McCollough CH, Vetter RJ. Update on patient radiation doses at a large tertiary care medical center. Health Phys 2001;81:530–5.
31. Radiation dose to patients from radiopharmaceuticals: A report of Committee 3 adopted by the International Commission on Radiological Protection. Ann ICRP 1991;22:1–18.
32. Bonow RO, Bennett S, Casey DE Jr., Ganiats TG, Hlatky MA, Konstam MA, et al. ACC/AHA clinical performance measures for adults with chronic heart failure: a report of the American College of Cardiology/American Heart Association Task Force on Performance Measures (Writing Committee to Develop Heart Failure Clinical Performance Measures) endorsed by the Heart Failure Society of America. J Am Coll Cardiol 2005;46:1144–78.
33. Radford MJ, Arnold JM, Bennett SJ, Cinquegrani MP, Cleland JG, Havranek EP, et al. ACC/AHA key data elements and definitions for measuring the clinical management and outcomes of patients with chronic heart failure: a report of the American College of Cardiology/American Heart Association Task Force on Clinical Data Standards (Writing Committee to Develop Heart Failure Clinical Data Standards): developed in collaboration with the American College of Chest Physicians and the International Society for Heart and Lung Transplantation: endorsed by the Heart Failure Society of America. Circulation 2005;112:1888–916.
34. Swedberg K, Cleland J, Dargie H, Drexler H, Follath F, Komajda M, et al. Guidelines for the diagnosis and treatment of chronic heart failure: executive summary (update 2005): The Task Force for the Diagnosis and Treatment of Chronic Heart Failure of the European Society of Cardiology. Eur Heart J 2005;26:1115–40.
35. Nieminen MS, Bohm M, Cowie MR, Drexler H, Filippatos GS, Jondeau G, et al. Executive summary of the guidelines on the diagnosis and treatment of acute heart failure: the Task Force on Acute Heart Failure of the European Society of Cardiology. Eur Heart J 2005;26:384–416.
36. Hunt SA. ACC/AHA 2005 guideline update for the diagnosis and management of chronic heart failure in the adult: a report of the American College of Cardiology/American Heart Association Task Force on Practice Guidelines (Writing Committee to Update the 2001 Guidelines for the Evaluation and Management of Heart Failure). J Am Coll Cardiol 2005;46:e1–82.